Earth and Planetary Science Letters 576 (2021) 117199

Contents lists available at ScienceDirect

Earth and Planetary Science Letters

www.elsevier.com/locate/epsl

Geomorphologic exploration targets at the Zhurong landing site in the southern Utopia Planitia of Mars

Binlong Ye [a,1], Yuqi Qian [b,1], Long Xiao [b,*], Joseph R. Michalski [a,*], Yiliang Li [a], Bo Wu [c], Le Qiao [d]

[a] Department of Earth Sciences and Laboratory for Space Research, University of Hong Kong, Hong Kong, China
[b] State Key Laboratory of Geological Processes and Mineral Resources, School of Earth Sciences, China University of Geosciences, Wuhan, China
[c] Department of Land Surveying and Geo-Informatics, The Hong Kong Polytechnic University, Hung Hom, Kowloon, Hong Kong, China
[d] Shandong Key Laboratory of Optical Astronomy and Solar-Terrestrial Environment, School of Space Science and Physics, Shandong University, Weihai, China

ARTICLE INFO

Article history:
Received 21 June 2021
Received in revised form 30 August 2021
Accepted 5 September 2021
Available online xxxx
Editor: W.B. McKinnon

Keywords:
Mars
missions
climate
rover

ABSTRACT

On May 15, 2021, Tianwen-1's rover Zhurong landed successfully at 109.926°E, 25.066°N, in southern Utopia Planitia on Mars. The Zhurong landing site contains a wide range of geomorphic exploration targets including troughs, raised ridges, pitted cones, mesas, sand dunes and crater ejecta. Aspects of all of these features suggest formation through interactions between volatiles, sediments, and magma. Pitted cones are invaluable windows into the subsurface and intriguing astrobiology targets for Martian life considering that they potentially formed from diapiric upwelling of fine-grained sediments (*i.e.* mud volcanism), a process that on Earth is often associated with methane release. The ground-penetrating radar onboard Zhurong will provide fundamentally new perspectives on the presence, distribution, and abundance of subsurface water-ice, a strategic natural resource for future crewed Mars exploration.

1. Introduction

China's first Mars probe Tianwen-1 entered orbit around Mars in March 2021. Unlike previous missions, it is the first-ever Mars expedition to deploy an orbiter, lander, and rover at one time (Ye et al., 2017; Li et al., 2021; Zou et al., 2021). Tianwen-1's rover Zhurong, landed successfully at 109.926°E, 25.066°N on May 15, 2021 (UTM+8), in southern Utopia Planitia in the northern plains of Mars (Fig. 1).

The Vastitas Boreals Formation (VBF), which is among the largest units on Mars and covers nearly 1/8 of the Martian surface (Tanaka et al., 2003, 2005, 2014), comprises much of the Zhurong landing region. The origin of the VBF remains enigmatic; it might be an early oceanic deposit (Carr and Head, 2003; Parker et al., 1989, 1993) but in any case likely represents aqueous sedimentary materials that sourced from outflow channels with contributions from highland and lowland sources (ABVi unit; Tanaka et al., 2014). The age of the Zhurong landing region including the VBF and other volcanic and sedimentary deposits in this area is Late Hesperian (c.a. 3.1 Gyr, Fig. 2) (Ivanov et al., 2014, 2017), though these materials have undergone long-term volcanic, fluvial, aeolian, periglacial and glacial modifications since their formation. Owing to the long and complex geological history, diverse types of geomorphological features have formed around the Zhurong landing site, including troughs, raised ridges, pitted cones, mesas, sand dunes and various crater ejecta deposits; some of them are driven by ice-related processes. Many units and structures in a larger area have been described in previous studies (e.g., McGill and Hills, 1992; Hiesinger and Head, 2000; Ivanov et al., 2014, 2015, 2017; Tanaka et al. 2003, 2005; Costard et al., 2016; Séjourné et al., 2019; Soare et al., 2020) and this study therefore focuses on the Zhurong landing region.

Instruments onboard Zhurong, such as the Multispectral Camera (MSCam), Mars Surface Composition Detector (MarSCoDe) and Mars Rover Penetrating Radar (RoPeR), could be used to study the in-situ features visually, geochemically, and geophysically. Exploration of Zhurong's landing site will be able to achieve the scientific goals of the Tianwen-1 mission (Li et al., 2021; Wu et al., 2021; Zou et al., 2021). Now that the exact landing site of the rover has been established, we here analyze the geomorphology of the site and describe scientific targets of opportunity that are accessible to the rover directly. High priority targets

* Corresponding authors.
E-mail addresses: longxiao@cug.edu.cn (L. Xiao), jmichal@hku.hk (J.R. Michalski).
[1] Binlong Ye and Yuqi Qian contributed equally to this work.

https://doi.org/10.1016/j.epsl.2021.117199
0012-821X/

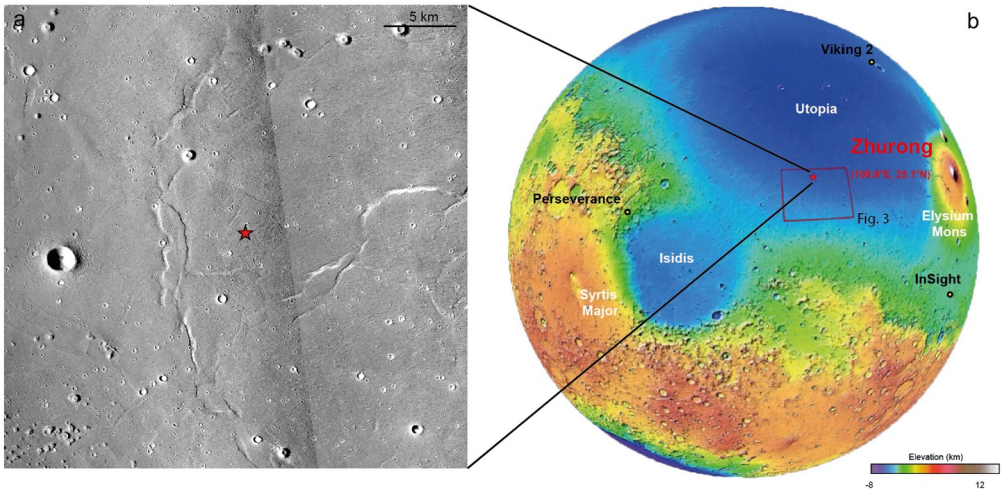

Fig. 1. (a) CTX images show Zhurong's landing site. The red star marks the location of the Zhurong Lander (CTX image ID: F04_037533_2068_XN26N250W and D22_035786_2060_XN_26N250W). (b) The geologic context of Zhurong's landing region. The red rectangle indicates the geomorphology mapping area of Fig. 3. The background is the MOLA colored shaded relief topographic map of Mars.

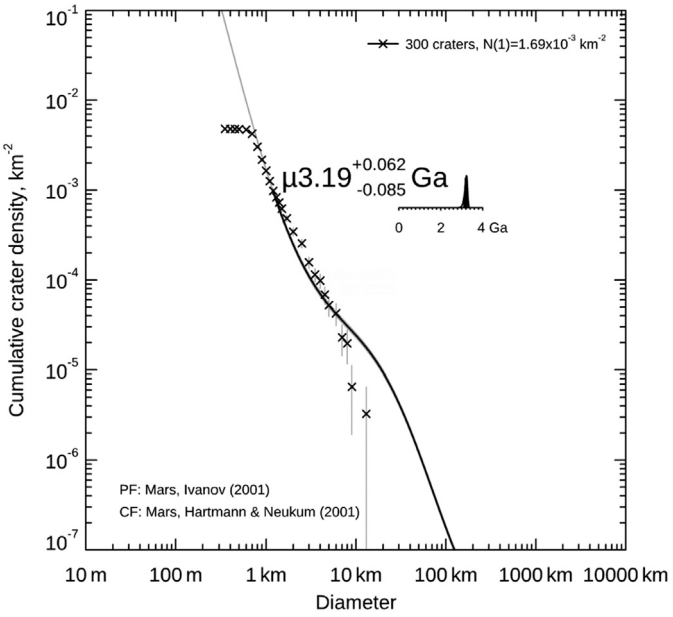

Fig. 2. Cumulative crater frequency plots are shown along with the model-fit and isochron for Zhurong landing region.

include putative mud volcanoes of great astrobiological interest and mapping of underground water-ice as strategic natural resources.

2. Methods

Data from NASA's Mars Reconnaissance Orbiter (MRO) Context Imager (CTX, 6 m/pixel) corrected mosaics (Dickson et al., 2018), and MRO High Resolution Imaging Science Experiment (HiRISE, 0.3 m/pixel) data (McEwen et al., 2007) were used to characterize geomorphological features of the Zhurong landing site. Gridded topographic data from NASA's Mars Global Surveyor (MGS) Mars Orbiter Laser Altimeter (MOLA) allow quantitative topographic analysis at 463 m/pixel (Smith et al., 2001). The Ames Stereo Pipeline (ASP) was used to generate CTX and HiRISE digital elevation models (DEMs) (Beyer et al., 2018). We also aligned the CTX-derived DEMs to MOLA PEDR data to improve the accuracy of DEMs (Mayer and Kite, 2016). In this study, a total of 3 CTX DEMs and 2 HiRISE DEMs were made to conduct quantitative morphology and morphometric analyses (Table S1).

Image and topographic data were integrated into a Geographic Information System (ArcGIS). Based on the texture and relief of the landing region, a variety of landforms were identified in the CTX images, including troughs, raised ridges, pitted cones, mesas, and various crater ejecta deposits. Pitted cones, mesa and domes were mapped as point data. Cones exhibit diverse spatial distribution patterns and at least three inter-connected examples that merged into one chain-like structure. Linear morphologic features, troughs and ridges, were only mapped as line features if longer than 500 m to improve the map clarity. Impact craters smaller than 1 km were not mapped. Crater counts were performed on CTX images using Cratertools within ArcMap (Kneissl et al., 2011). Crater counts were calculated using Craterstats2, which determines the best model age based on the nonlinear least-squares fit to cumulative crater size-frequency distribution over a given range of crater diameters (Michael and Neukum, 2010). Model age determination is made using the production function of Ivanov (2001) and chronology function of Neukum et al. (2001).

3. Results

The Zhurong landing region, located in the southern part of Utopia Planitia west of the Elysium volcanic province (Wan et al., 2020; Wu et al., 2021) is topographically smooth and low in elevation. We selected a ~710 km × 470 km rectangle as the study area (top-left corner: 104°E, 28°N, lower-right corner: 116°E, 20°N, Fig. 1b) because this area provides the context of the precise landing spot and includes all of the geologic features that could conceivably be visited by the rover. Examples of intriguing landforms, such as troughs, raised ridges, pitted cones, mesas, and different types of crater ejecta are shown in Fig. 3.

More than 4000 cones were identified in the study region (Fig. 6). Those cones consistently have a smooth surface texture relative to the adjacent ground and a central depression on the summit (Fig. 4). The summit crater diameters are about 50% of the cone base size and the slopes along the flanks of cones are 15°–20°. These features show different preservation states: some cones are intact (Fig. 3a and Fig. 4) while others are partly breached and eroded on the downslope margins by the formation of irregular, crescent-shaped edifices (Fig. 5). Locally, some cones appear in chains (Fig. 3b), and some cones are distributed in clusters rather than sporadically (Fig. 3c). The cone chains generally

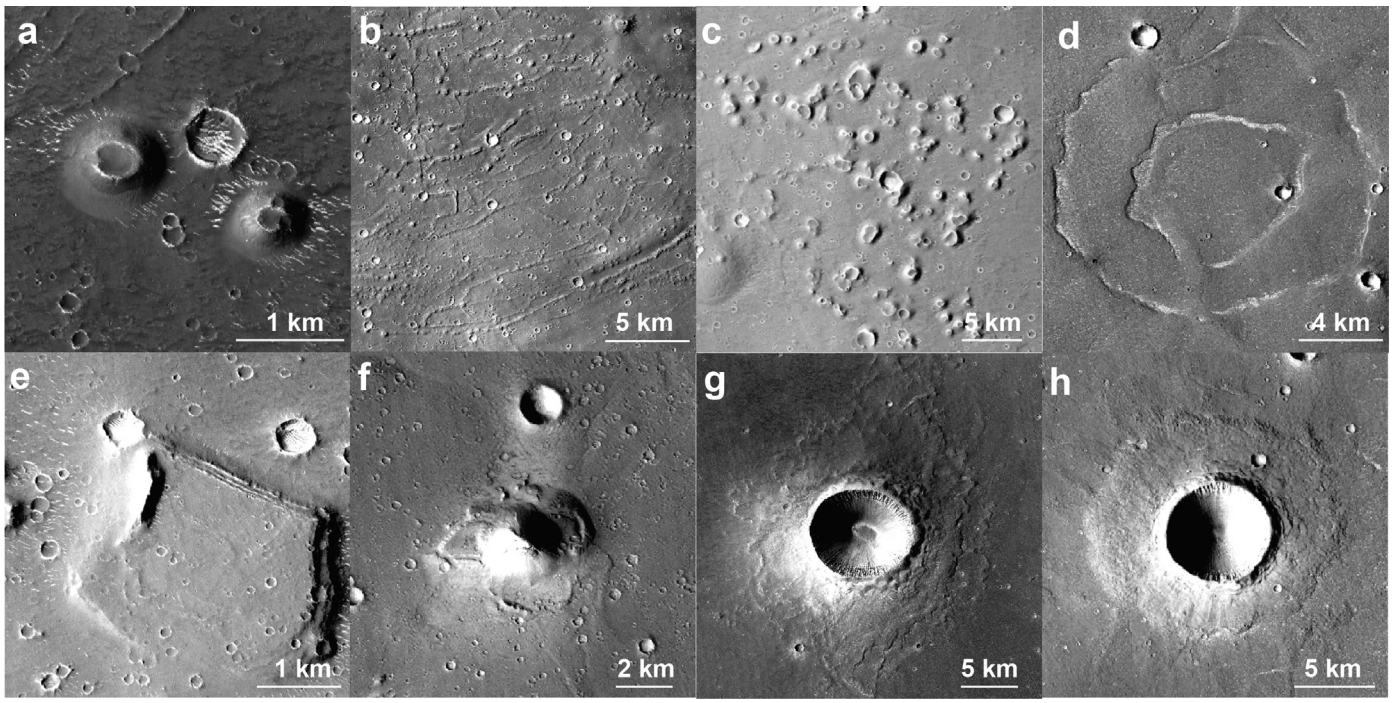

Fig. 3. CTX and HiRISE images show varied landforms near the Zhurong landing site: (a) pitted cones (110.26°E, 25.4°N; ESP_043896_2055), (b) pitted cone chains (105.45°E, 22.50°N; CTX), (c) cone clusters (106.2°E, 24.12°N; CTX), (d) troughs (112.51°E,27.32°N; CTX), (e) mesas (105.5°E, 22.3°N; CTX), (f) domes (113.43°E,23.45°N; CTX), (g) rampart craters (107.26°E, 24.26°N; CTX), (h) pancake-like ejecta (112.30°E, 27.32°N; CTX). The CTX mosaic product of Dickson et al. (2018) is available at this website (http://murray-lab.caltech.edu/CTX/).

occur on lobed features within the VBF (Fig. 3b). We measured the diameter and height of 130 cones using CTX DEMs. The base width of cones varies from 200 m to 1100 m, with an average size of 615 m. Their heights range from 10 to 100 m with a mean value of 30 m. The summit crater diameters are about 50% of the cone base size and the slopes along the flanks of pitted cones are 15–20° (Table S2).

Linear or polygonal troughs dominate the northern part of the mapping region (Fig. 6). The length of these troughs varies from 0.4–50 km and the width of troughs ranges from ~100 m to 1000 m. Some fractures exhibit near-circular shapes in map view (Fig. 3d), which has been interpreted as evidence of "ghost craters" or circular graben (Ivanov et al., 2017; Buczkowski et al., 2012; Cooke et al., 2011). These troughs were likely formed by tectonic uplift and extension of Utopia basin following sublimation of an ice-rich substrate (Hiesinger and Head, 2000) or volumetric compaction (Buczkowski et al., 2012). The geospatial relationships among these troughs and pitted cones are interesting (Fig. 6): troughs appear pervasively in the northeast mapping region while the pitted cones are dominantly distributed in the southwest. Troughs are prevalent central Utopia basin to the north, and only a few spots show pitted cones there (Fig. 7a). The rover fortuitously landed near the boundary of a geomorphological transition from trough forming to cone-forming processes.

Narrow and raised ridge segments are also observed in the landing region (Fig. 7). These ridge segments are either linear or curving, and some linear features are emplaced in an en echelon pattern. These ridges generally have a rough and uneven, but symmetrical surface texture (Fig. 7c). There are up to 150 ridges observed with a mean length of 3 km and a maximum length of ~36 km (Fig. 7a). MOLA profiles show that individual ridges have heights varying between 10–20 m.

The morphology of the impact craters provides additional insight into surface or subsurface properties. The multiple-layered ejecta of some craters changes from rampart (Fig. 3g) termini to pancake-like ejecta (Fig. 3h) with the increased latitude, consistent with previous studies (Tanaka et al., 2003; Ivanov et al., 2014, 2015). Such ejecta patterns have been interpreted to be caused by volatiles in the substrate (Carr et al., 1977; Barlow, 2005; Mouginis-Mark, 1979), and the change in morphology with latitude might therefore indicate the change in volatile content of the substrate with latitude.

Flat-topped mesas or mounds (Fig. 3e) are morphologically distinct from the cones. The albedo of mounds is akin to their surrounding terrains. These mounds are 2–10 km in diameter and about 150–200 m in height. Locally, some mounds show layering or terrancing in their exposed flanks (Fig. 3e). We also observed some large domes on these mesas that differ from pitted cones (Fig. 3f). These mesas appear to represent erosional remnants of previous terrains (Ivanov et al., 2014).

4. Discussion

4.1. The origin of the pitted cones

A variety of mechanisms has been proposed for the formation of pitted cones on Mars including interpretations as mud volcanoes (Brož et al., 2019; Hemmi and Miyamoto, 2017; Ivanov et al., 2014, 2015; Komatsu et al., 2016), rootless cones (Hamilton et al., 2011; Noguchi and Kurita, 2015), cinder/scoria cones (Brož et al., 2015; Meresse et al., 2008), tuff cones/rings (Brož and Hauber, 2013), and pingos (de Pablo and Komatsu, 2009; Dundas et al., 2008; Dundas and McEwen, 2010). These different hypotheses have drastically different implications for geology, magmatic processes, and astrobiology on early Mars.

Our morphometric data in the rover landing region provide additional constraints on the origin of pitted cones. Height/diameter data for the pitted cones in this area measured from high resolution DEMs provide a larger dataset than what has been presented previously (e.g., Skinner and Tanaka, 2007). Though the sizes of pitted cones around the Zhurong landing site are smaller than some

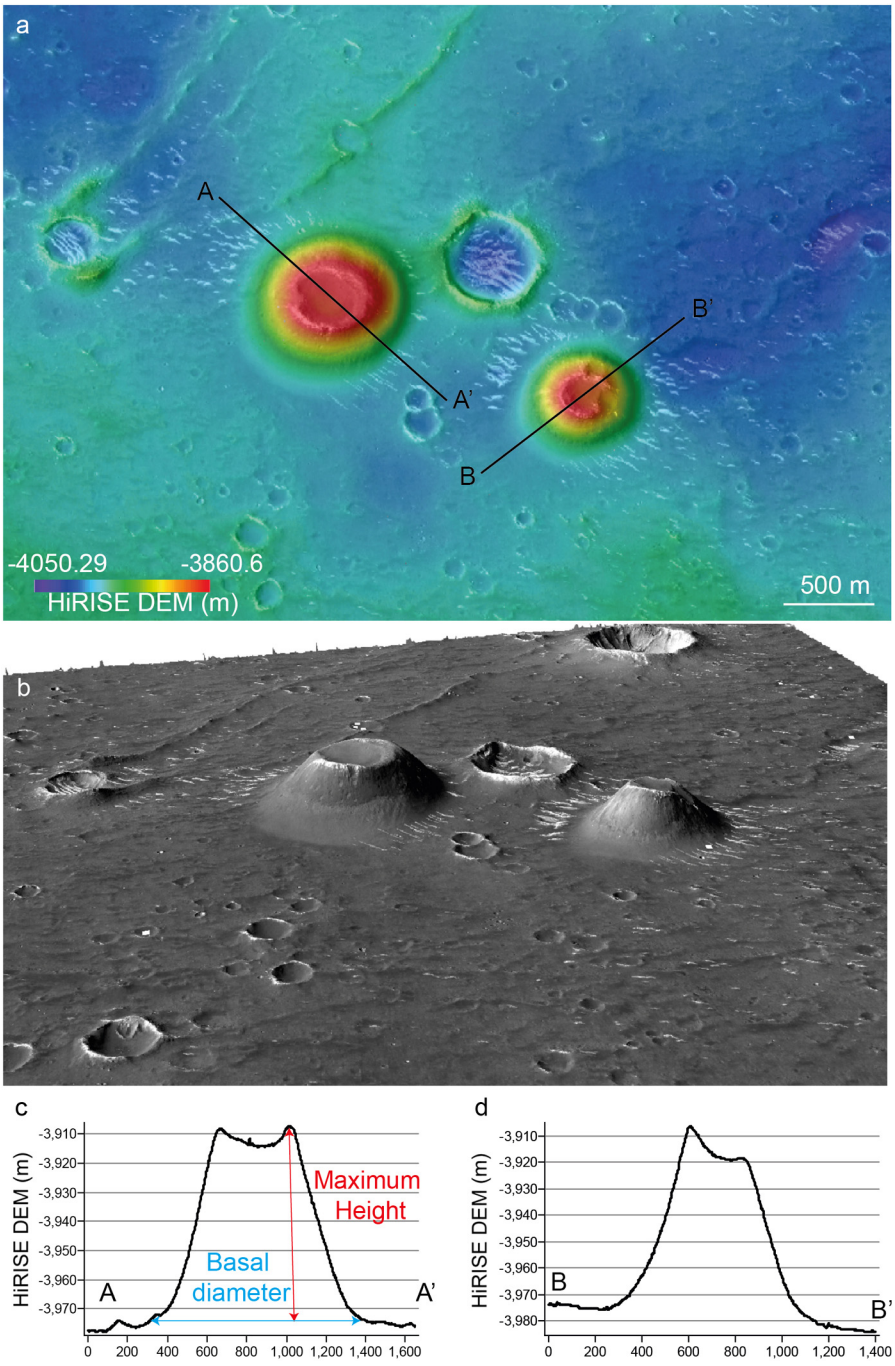

Fig. 4. a) HiRISE topography data are draped over HiRISE images to show the morphology and topography of pitted cones in the landing region. This figure also shows how to measure maximum height and basal diameter. b) A perspective view of pitted cones (3x vertical exaggeration). c–d) HiRISE topographic profiles are shown for two small pitted cones. DEM is ESP_044885_2055_ESP_043896_2055.

terrestrial mud volcanoes, they show similar relationships when comparing height/basal aspect ratios (Fig. 8c). These cones are also similar in scale to other putative mud volcanoes on Mars (Hemmi and Miyamoto, 2017; Komatsu et al., 2016). The basal diameter and height of the scoria/cinder cone and tuff rings/cones on Earth and Mars elsewhere are significantly larger than the pitted cones on Utopia Planitia (Fig. 8b). The height/basal diameter ratios of scoria/cinder cones are larger than the cone features measured here, while tuff rings/cones are lower. Rootless cones are a few orders of magnitude smaller than the cones discussed here. A comparison of the morphology of the pitted cones also supports the mud volcano origin hypothesis. In other localities, rootless cones are generally associated with lava flows and have raised rims along the edges of summit pits (Noguchi and Kurita, 2015), which is not the case of the pitted cones.

Pingos are common periglacial landforms that develop by freezing pressurized groundwater, which fits the geological context of this region. Height/diameter morphometrics for pingos are similar to those of the pitted cones, but a distinction between pingos and pitted cones in the landing zone is made here based on morphological details. Previous works have reported that the occurrence of pingos in central Utopia (between 35–45°N) at relatively high latitudes, but they generally are flat-topped mounds with meter-scale polygonal troughs or cracks on the surface and have textures similar to those within the background terrain (Dundas et al., 2008; Dundas and McEwen, 2010). In addition, pingoes typically

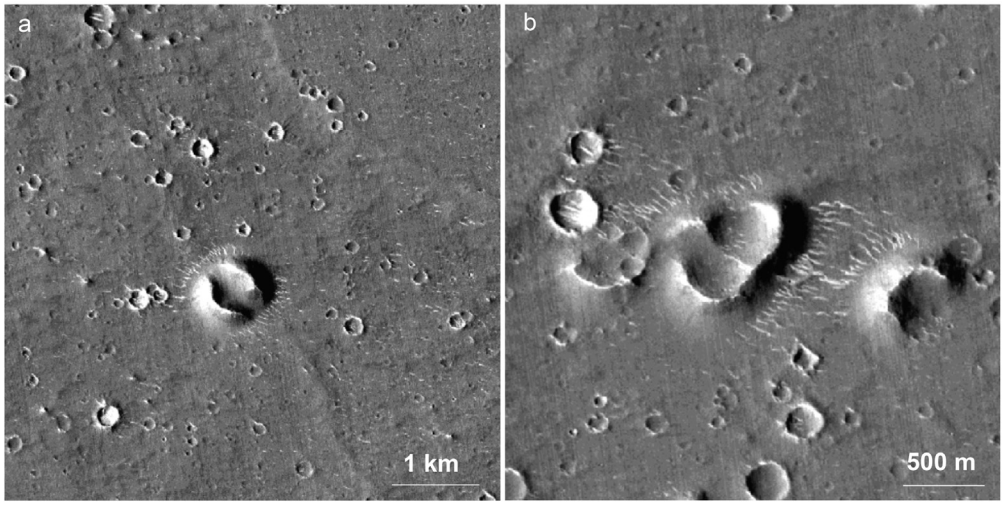

Fig. 5. CTX images show different preservation states of pitted cones. (a: 108.35°E, 25.23°N, b: 108.28°E, 25.23°N).

have fractures at their summits, features that are not observed for the Zhurong site pitted cone polulations. In the case of mud volcanism, the cones form by upward transport of fluid and fine-grained sediment from the subsurface. Pingos form by the freezing of groundwater, development of subsurface ice lenses, and subsequent increase in bulk volume, leading to the uplift of the surface. Therefore, pingos are uplifted terrain and mud volcanoes are effusive sediment. The margins of pingo should therefore show gradual transitions into the surrounding materials while mud volcanoes should show geologic contacts with the terrain in which they occur. Our observations of sharp contacts between pitted cone edges and the surrounding terrain support the mud volcano hypothesis (Fig. 4b).

We also compared boulders around pitted cones and surrounding impact craters in order to evaluate rockiness and estimate grain size of the cone material. The pitted cones show fewer boulders than the surrounding impact craters (Fig. 9). It indicates that cones are composed of different material than the surrounding substrate and that cone materials are relative finer grained and/or less competent compared to the surrounding units. The fine-grained and soft sediment around pitted cones is in our view most consistent with a mud volcano interpretation, but it is clear that multiple working hypotheses should be carried forward.

Most pitted cones occur in the south of the mapped area whereas troughs appear in the north (Fig. 6). If these pitted cones are pingos, it does not explain why they occur preferentially at lower latitutes, where water-ice might be less abundant. The formation of troughs likely involved sublimation of ice (Hiesinger and Head, 2000; Ivanov et al., 2014). This spatial correlation could partly be explained by the latitude-dependent water-ice abundance, thickness or possibility for melting, but the geomorphologic transition boundary is not a straight line along the latitude. Instead, it follows the topographic change of the basin, implying the topography plays an important role in affecting the distribution of the landforms and perhaps the sediments and ice as drivers of landform development.

It is possible that once the permafrost layer formed, it prevented subsurface fluidized sediments from emerging to form mud volcanoes. The correlation of landforms with what is likely the occurrence of ice, depth to ice, or ice abundance could therefore support a “volcanic” origin driven by volatiles and would be inconsistent with traditional volanism driven soley by magma in most cases.

Landforms in the region are diverse, however, and there is a possibility that some structures formed by volatile release and others formed by magmatism/volcanism. In the north, pitted cones are rare, but there is one place where raised ridges and cones are found together (Fig. 7). These ridges strikingly resemble dike swarms found in eastern Utopia Planitia (Pedersen et al., 2010), suggesting a possible genetic link. The putative dike swarms were potentially emplaced subglacially or within an ice-rich sedimentary deposit. Their morphology has been interpreted to be analogous to moberg ridges on Earth (Chapman, 1994; Pedersen et al., 2010). The co-occurrence of pitted cones and ridges indicates there is a causal link between mud volcanoes and potential dike swarms in the center of the Utopia basin. The magma chamber which fed these dike swarms could have also been a heat source for maintaining the mobility of the mud reservoir and groundwater system. Therefore, we might expect additional mud volcanoes associated with dikes elsewhere in the north.

Furthermore, outflow channels on ancient terrains of Mars have been interpreted as products of catastrophic flood events and the major water source for the putative northern ocean (Tanaka et al., 2003; Ivanov et al., 2014, 2015). Whether or not a large, stable ocean formed, it is perhaps inescapable that deluges of water and sediment/slurry would have been deposited in the plains of Utopia Planitia periodically. The rapid burial of aqueous sediments after these events could have fed an enormous mud reservoir around the Utopia basin and provided favorable conditions for sediment upwelling (Mazzini and Etiope, 2017).

4.2. Geology, climate, and astrobiology

On Earth, mud volcanoes are an important source of methane release into the atmosphere and contributed ∼12% to the preindustrial methane budget (Mazzini and Etiope, 2017; Oehler and Etiope, 2017). Mars Express observations have shown local methane enrichments in the atmosphere above Syrtis Major/Terra Sabae (Formisano et al., 2004). Mud volcanoes are a promising target to look for the source of current atmospheric methane of Mars (Oehler and Etiope, 2017).

Methane in terrestrial mud volcanoes generally form in three ways: (a) biogenic, (b) thermogenic, and (c) migration from deep methane reservoirs (Oehler and Etiope, 2017). The methane released by most mud volcanoes on Earth is nearly thermogenic, as the product of the breakup of organic matter at elevated temperatures and pressures in deep-buried sedimentary strata (Oehler and Etiope, 2017). This process has been considered biotic and gener-

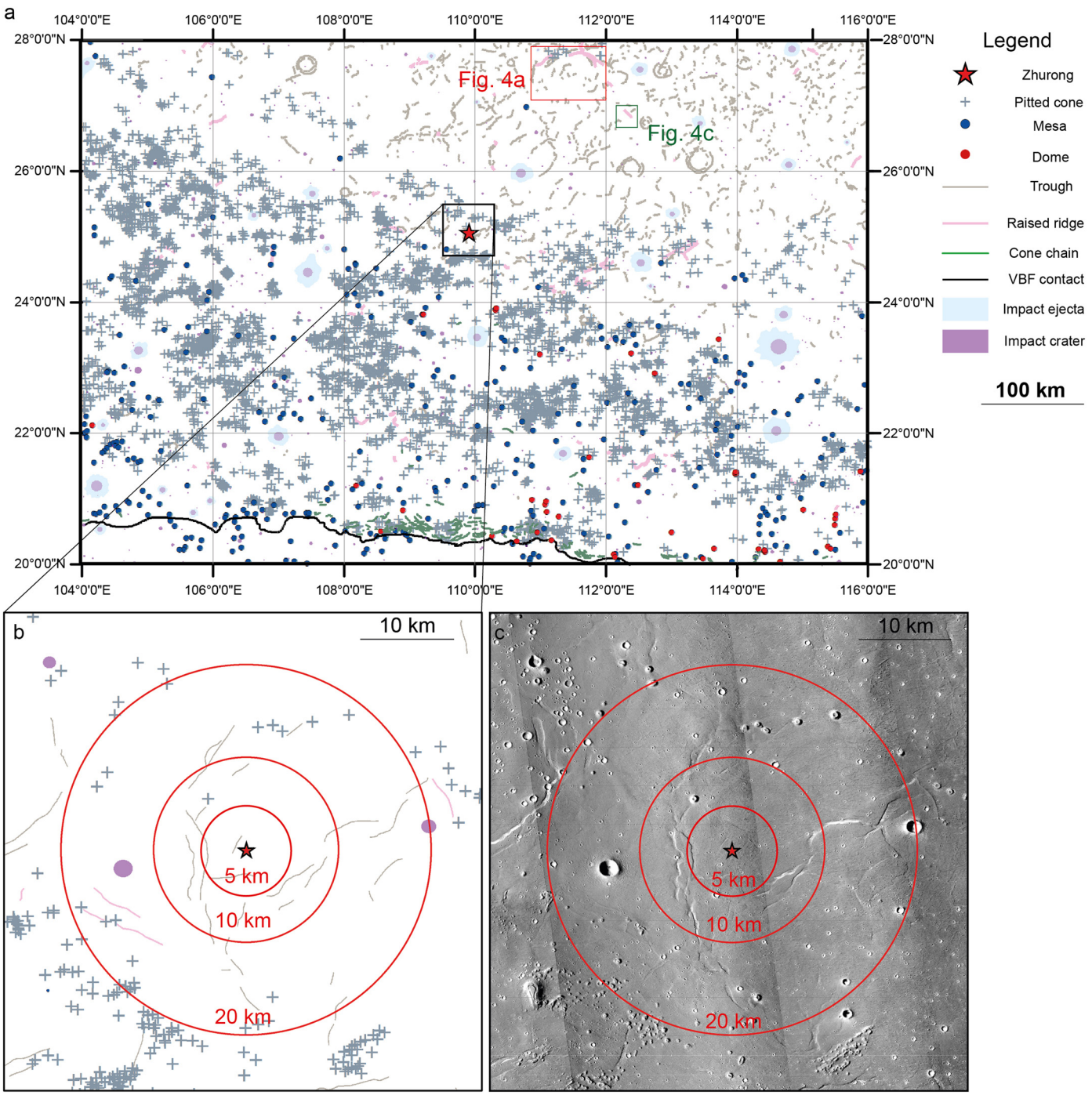

Fig. 6. (a) The distribution of morphologic features in the study area. VBF contact is from Ivanov et al. (2017). Colored rectangles show the location of Fig. 7a and Fig. 7c, respectively. (b) Close-up view of morphogic features map of Zhurong landing region. (c) CTX mosaic of the enlarged morphology map (CTX image ID: F04_037533_2068_XN26N250W and D22_035786_2060_XN_26N250W). Concentric circles centered on the landing site, with their radii labelled, are shown in panels b and c, to describe the rover traverse mobility.

ally associated with microbial life on Earth (Niemann et al., 2006). Therefore, the presence of methane is of great astrobiological interest, bearing clues of prebiotic biosignatures or evidence of life, although abiotic processes could also explain its origin.

Benzene and propane have been discovered the Gale crater (Eigenbrode et al., 2018) within a 3 Ga old sedimentary rock, which opens the possibility of the preservation of organic molecules in the ancient sediments of Utopia basin. Organic molecules could form on Mars through prebiotic reactions in-situ or be delivered by meteorites and interplanetary dust particles (IDPs) (Flynn, 1996). It is estimated that up to 3 km of sediment has been deposited in Utopia (Cooke et al., 2011) and this material could potentially have brought with it organic material from the highlands.

In addition, methane is one of the most powerful greenhouse gases, and may have had a significant impact on ancient climate (Liu et al., 2021). Huge amounts of methane hydrate (clathrate), a form of crystalline water that traps methane inside their structure, has been found on the seafloor and permafrost on Earth (Sloan and Koh, 2007). Likewise, clathrates might be stored in the subsurface

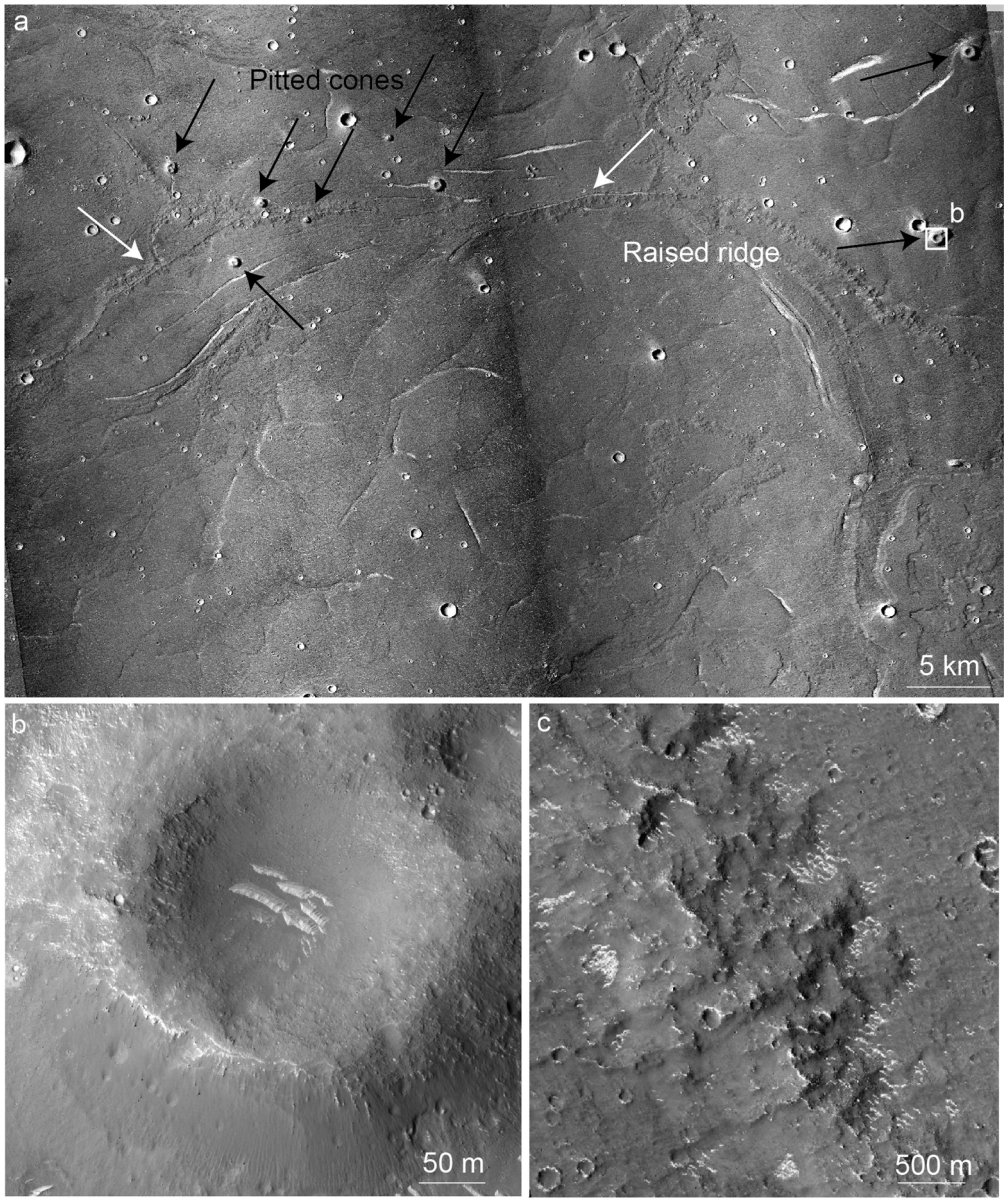

Fig. 7. (a) A CTX mosaic shows the distribution of raised ridges and pitted cones. The black arrows show pitted cones while the white arrows indicate raised ridges. (b) A close-up view of a pitted cone shows a smooth surface texture (HiRISE image ID: ESP_036709_2080). (c) The high-resolution image illustrates the rough and uneven ridge surface (HiRISE image ID: ESP_035865_2070).

and their abrupt release could be the trigger of short-tern climate excursions on early Mars (Kite et al., 2017) (Fig. 10).

4.3. Guide for the future mission planning

The subsurface of Mars might be the best place to search for biosignatures and evidence of life because it would provide shelter from deleterious radiation, energy, and liquid for life emerging and survival (Michalski et al., 2018). But until now, it's not feasible to deploy drilling on Mars to access deep subsurface materials. The upcoming ExoMars rover will be equipped with a drilling system, but can only sample to 2 m deep within clay-bearing materials in best case conditions. Mud volcanoes on Earth, generally expel subsurface materials from several hundreds of meters deep, including fluidized sediments and gas (Mazzini and Etiope, 2017; Brož et al., 2019). Potential mud volcanoes within the landing region therefore provide a unique natural probe to collect deep subsurface materials, which might offer a valuable glimpse of prebiotic chemistry, evidence of life, and clues to a possible thriving deep biosphere beneath the cold and desolate surface. The combination of Multispectral Camera (MSCam) data and Mars surface Composition Detector (MarsCoDe) data will enable characterization of fine-scale morphology, texture, and composition of deposits associated with cones and could distinguish between multiple working hypotheses for these features (Li et al., 2021; Zou et al., 2021). Currently, Zhurong is heading south from the landing site. The closest cone, if the rover continues in this direction, is 15 km away at the time of this writing (Fig. 1). Cones should be among the priority targets for exploration and could be reachable considering a maximum drive speed up to 200 m per hour (Yuan et al., 2021) might be achievable over parts of the extended mission. Among the most accessible targets along the way will be sand dunes of various forms and albedo, the analysis of which will shed light on recent atmospheric conditions and climate (Thomas et al., 1999).

A top priority of current exploration is to identify accessible ice resources as close to the surface as possible (Morgan et al., 2021). Water-ice was found in the very shallow subsurface be-

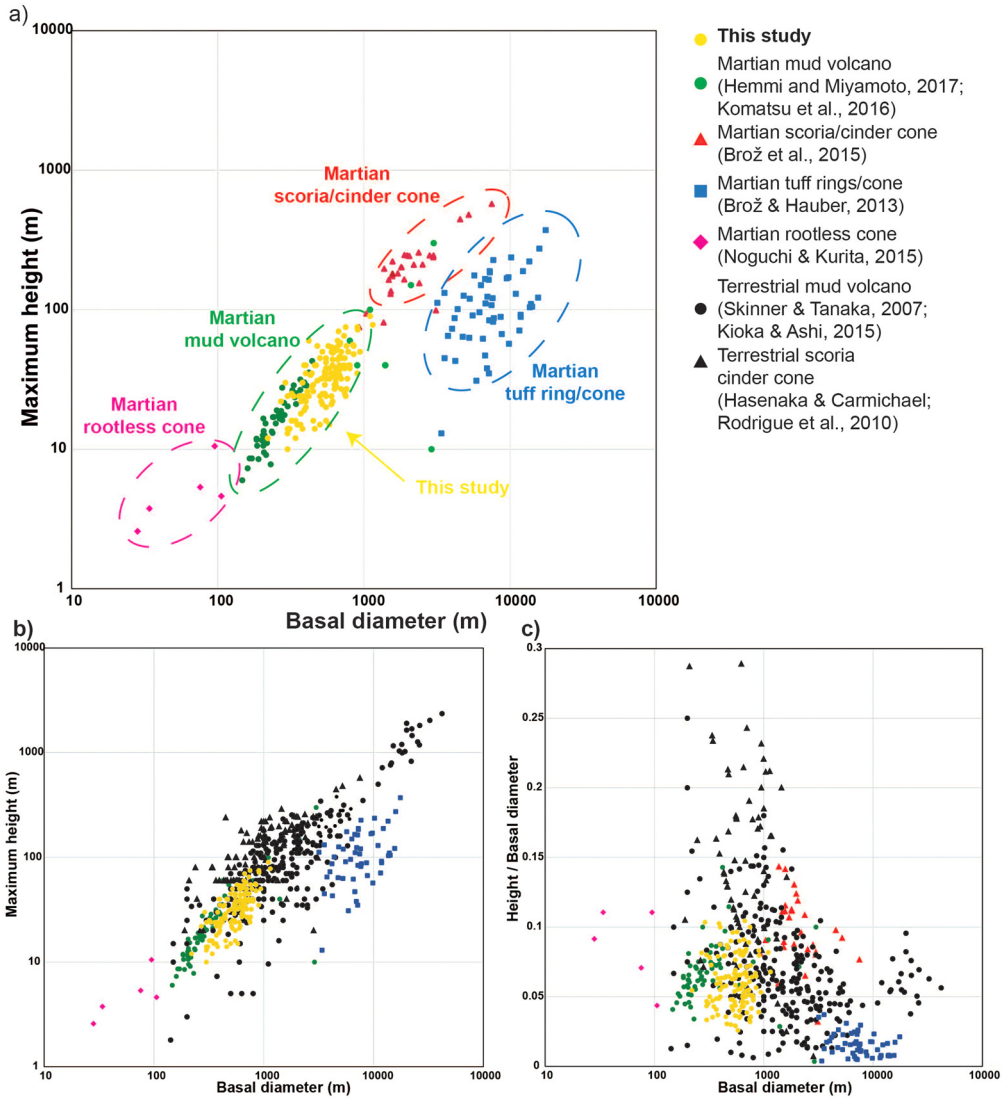

Fig. 8. a) Morphometric comparison between the pitted cones measured by this study and previous reports. Log-log plots show maximum cone height versus basal diameter. Data of morphometric measurements of pitted cones from this study are available in Table S2. b) Log-log plots show maximum cone height versus basal diameter including terrestrial cinder cones and mud volocanos data. c) Aspect ratio (height/basal diameter) versus basal diameter. Data for possible martian scoria cones are from Brož et al. (2015). Data for possible martian mud volcanoes in Terra Sirenum and in Chryse Planita, are from Hemmi and Miyamoto (2017), Komatsu et al. (2016), respectively, for martian rootless cones are from Noguchi and Kurita (2015), for possible martian tuff rings/tuff cones data are from Brož and Hauber (2013), for terrestrial cinder cones, are from Hasenaka and Carmichael (1985) and Rodríguez et al. (2010), and for terrestrial mud volcanoes are from Skinner and Tanaka (2007) and Kioka and Ashi (2015).

low the Phoenix lander (Smith et al., 2009) or through analyses of Gamma Ray data (Mitrofanov et al., 2004). In the Utopia Planitia region, subsurface water/ice has been inferred via observation by the SHARAD radar (Stuurman et al., 2016) and morphologic analysis (Morgan et al., 2021).

There are currently three satellite-borne radar instruments at Mars, including the MARSIS (Mars Express), SHARAD (Mars Reconnaissance Orbiter), and MOSIR (Tianwen-1). In theory, these orbiting radar instruments are able to detect reflection from up to 1 km deep of martian crust. But, echoes are most easily detectable only in ice-rich or volcanic ash (generally less than 100 m deep), which greatly limits our understanding of martian subsurface structure (Stillman and Grimm, 2011). The ground penetrating radar (RoPeR) onboard Zhurong (Zhou et al., 2020), would fill the gap between orbital and in-situ water-ice detection, offering a groundbreaking understanding of the presence, distribution, and abundance of subsurface water, a strategic natural resource.

Zhurong landed in a geologically and geomorphologically complex region of Mars, one which includes a transition among terrains with different feature types that are linked to multiple geologic processes likely related to ice occurrence and abundance, and therefore to climate evolution. Evaluation of exposed surface units and sounding of the subsurface with the capable scientific payload will undoubtedly shed new light on the subsurface structure of a type of terrain on Mars that has not been well explored in-situ. The exploration by Zhurong will undoubtedly further our understanding of the global geology, climate, and astrobiology of Mars, not only in terms of the geologic past and modern environment, but also in consideration of future strategic planning.

CRediT authorship contribution statement

Binlong Ye wrote the paper and carried out analyses. Yuqi Qian edited the paper and carried out analyses. Long Xiao provided geological discussions and edited the paper. Joe Michalski provided geological discussions and edited the paper. Yiliang Li, Bo Wu and Le Qiao helped edit the manuscript.

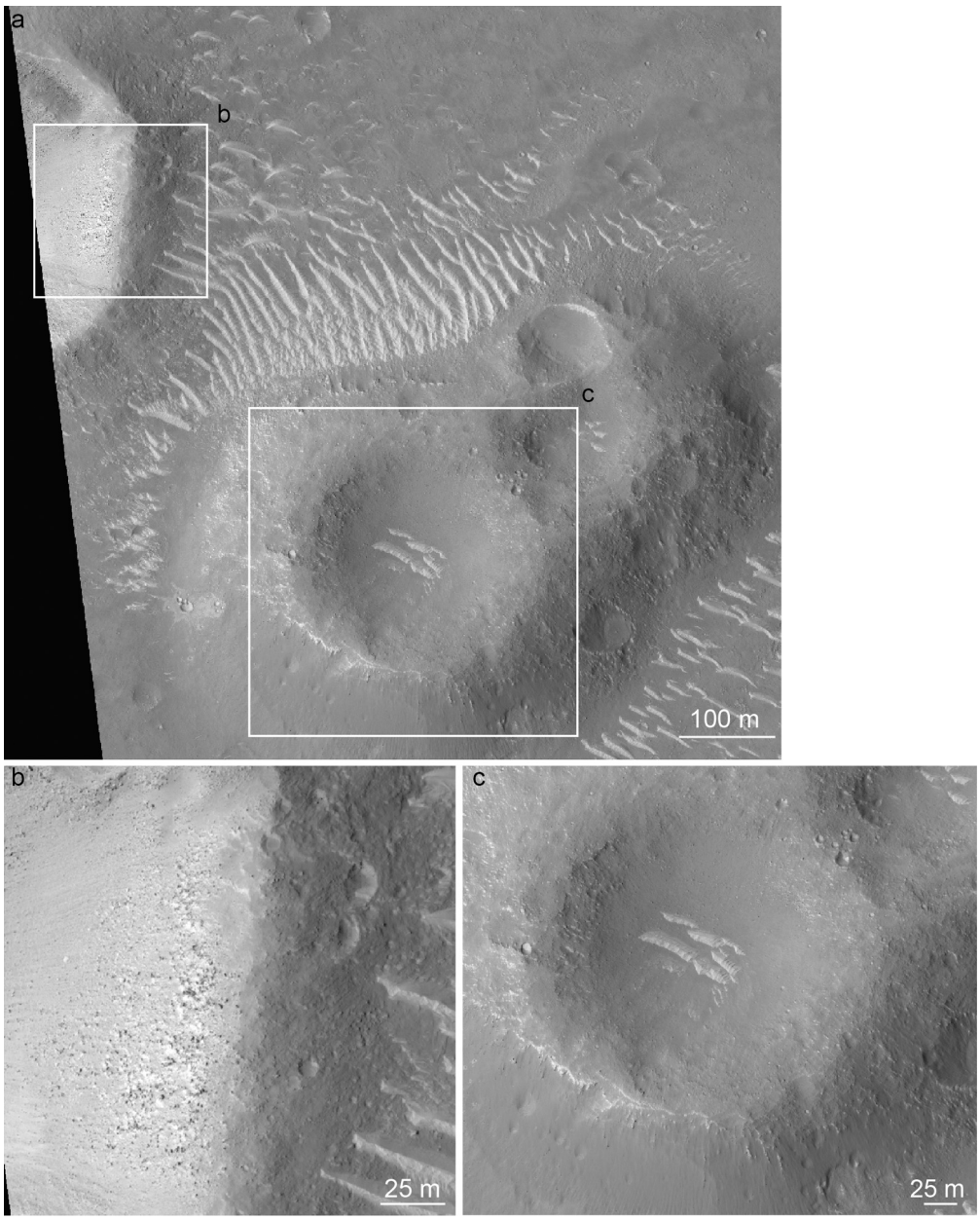

Fig. 9. (a) This figure shows boulders on the craters and the pitted cone. Close-up view of boulders on crater wall (b) and pitted cone (c), respectively (HiRISE ID: ESP_036709_2080).

Declaration of competing interest

The authors declare that they have no known competing financial interests or personal relationships that could have appeared to influence the work reported in this paper.

Acknowledgements

All data used in this paper are available in NASA Planetary Data System (pds.jpl.nasa.gov). We thank J. Dickson for building CTX mosaic data, which are available on this website (http://murray-lab.caltech.edu/CTX/). DEMs used in this study are available on the Digital Repository at The University of Hong Kong (doi:https://doi.org/10.25442/hku.15132480). The authors especially thank the editor William McKinnon, Chris Okubo and an anonymous reviewer for their feedbacks and insightful suggestions that improved the quality of this manuscript. Discussion with Gongbao Nan helped to understand deep-sea mud volcanoes and methane on Earth. L.X. and Y.Q. were supported by the Pre-research Project on Civil Aerospace Technologies of CNSA (No. D020101), National Natural Science Foundation of China (No. 41830214). L.Q. was supported by the Pre-research Project on Civil Aerospace Technologies of CNSA (No. D020102). J. Michalski and B. Ye were supported by the Hong Kong Research Grants Council Research Impact Fund Project No. R5043-19.

Appendix A. Supplementary material

Supplementary material related to this article can be found online at https://doi.org/10.1016/j.epsl.2021.117199.

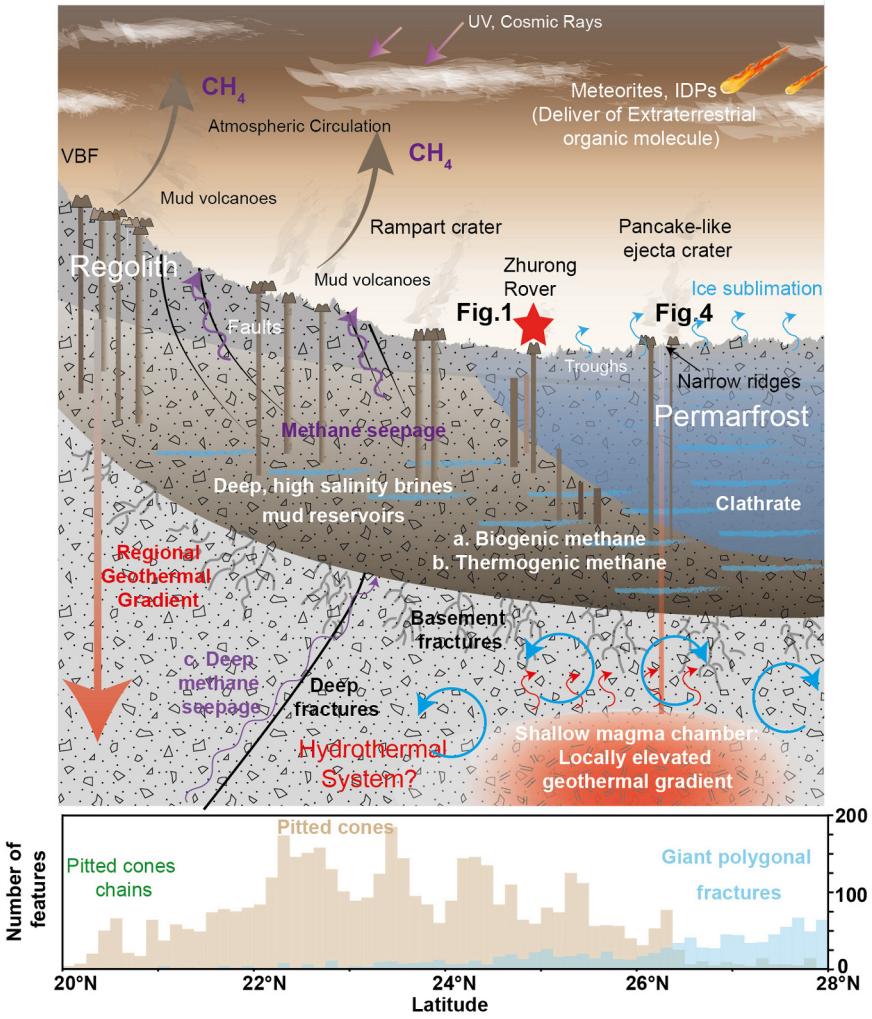

Fig. 10. A schematic cross-section shows ice, mud, and volcanism interaction in the past of the Zhurong landing region in Utopia Planitia.

References

Barlow, N.G., 2005. A review of Martian impact crater ejecta structures and their implications for target properties. In: Large Meteorite Impacts III, vol. 384, pp. 433–442.

Beyer, R.A., Alexandrov, O., McMichael, S., 2018. The Ames Stereo Pipeline: NASA's open source software for deriving and processing terrain data. Earth Space Sci. 5 (9), 537–548.

Brož, P., Hauber, E., 2013. Hydrovolcanic tuff rings and cones as indicators for phreatomagmatic explosive eruptions on Mars. J. Geophys. Res., Planets 118 (8), 1656–1675.

Brož, P., Čadek, O., Hauber, E., Rossi, A.P., 2015. Scoria cones on Mars: detailed investigation of morphometry based on high-resolution digital elevation models. J. Geophys. Res., Planets 120 (9), 1512–1527.

Brož, P., Hauber, E., Van de Burgt, I., Špillar, V., Michael, G., 2019. Subsurface sediment mobilization in the southern Chryse Planitia on Mars. J. Geophys. Res., Planets 124 (3), 703–720.

Buczkowski, D.L., Seelos, K.D., Cooke, M.L., 2012. Giant polygons and circular graben in western Utopia basin, Mars: exploring possible formation mechanisms. J. Geophys. Res., Planets 117 (E8).

Carr, M.H., Head III, J.W., 2003. Oceans on Mars: an assessment of the observational evidence and possible fate. J. Geophys. Res., Planets 108 (E5).

Carr, M.H., Crumpler, L.S., Cutts, J.A., Greeley, R., Guest, J.E., Masursky, H., 1977. Martian impact craters and emplacement of ejecta by surface flow. J. Geophys. Res. 82 (28), 4055–4065.

Chapman, M.G., 1994. Evidence, age, and thickness of a frozen paleolake in Utopia Planitia, Mars. Icarus 109 (2), 393–406.

Cooke, M., Islam, F., McGill, G., 2011. Basement controls on the scale of giant polygons in Utopia Planitia, Mars. J. Geophys. Res., Planets 116 (E9).

Costard, F., Séjourné, A., Kargel, J., Godin, E., 2016. Modeling and observational occurrences of near-surface drainage in Utopia Planitia, Mars. Geomorphology 275, 80–89.

de Pablo, M.Á., Komatsu, G., 2009. Possible pingo fields in the Utopia basin, Mars: geological and climatical implications. Icarus 199 (1), 49–74.

Dickson, J., Kerber, L., Fassett, C., Ehlmann, B., 2018. A global, blended CTX mosaic of Mars with vectorized seam mapping: a new mosaicking pipeline using principles of non-destructive image editing. Paper presented at the Lunar and Planetary Science Conference.

Dundas, C.M., McEwen, A.S., 2010. An assessment of evidence for pingos on Mars using HiRISE. Icarus 205 (1), 244–258.

Dundas, C.M., Mellon, M.T., McEwen, A.S., Lefort, A., Keszthelyi, L.P., Thomas, N., 2008. HiRISE observations of fractured mounds: possible Martian pingos. Geophys. Res. Lett. 35 (4).

Eigenbrode, J.L., Summons, R.E., Steele, A., Freissinet, C., Millan, M., Navarro-Gonzalez, R., et al., 2018. Organic matter preserved in 3-billion-year-old mudstones at Gale crater, Mars. Science 360 (6393), 1096–1100.

Flynn, G.J., 1996. The delivery of organic matter from asteroids and comets to the early surface of Mars. In: Worlds in Interaction: Small Bodies and Planets of the Solar System. Springer, pp. 469–474.

Formisano, V., Atreya, S., Encrenaz, T., Ignatiev, N., Giuranna, M., 2004. Detection of methane in the atmosphere of Mars. Science 306 (5702), 1758–1761.

Hamilton, C.W., Fagents, S.A., Thordarson, T., 2011. Lava–ground ice interactions in Elysium Planitia, Mars: geomorphological and geospatial analysis of the Tartarus Colles cone groups. J. Geophys. Res., Planets 116 (E3).

Hasenaka, T., Carmichael, I.S., 1985. The cinder cones of Michoacán—Guanajuato, central Mexico: their age, volume and distribution, and magma discharge rate. J. Volcanol. Geotherm. Res. 25 (1–2), 105–124.

Hemmi, R., Miyamoto, H., 2017. Distribution, morphology, and morphometry of circular mounds in the elongated basin of northern Terra Sirenum, Mars. Prog. Earth Planet. Sci. 4 (1), 26.

Hiesinger, H., Head III, J.W., 2000. Characteristics and origin of polygonal terrain in southern Utopia Planitia, Mars: results from Mars Orbiter Laser Altimeter and Mars Orbiter Camera data. J. Geophys. Res., Planets 105 (E5), 11999–12022.

Ivanov, B.A., 2001. Mars/Moon cratering rate ratio estimates. Space Sci. Rev. 96 (1), 87–104.

Ivanov, M.A., Hiesinger, H., Erkeling, G., Reiss, D., 2014. Mud volcanism and morphology of impact craters in Utopia Planitia on Mars: evidence for the ancient ocean. Icarus 228, 121–140.
Ivanov, M.A., Hiesinger, H., Erkeling, G., Reiss, D., 2015. Evidence for large reservoirs of water/mud in Utopia and Acidalia Planitiae on Mars. Icarus 248, 383–391.
Ivanov, M.A., Erkeling, G., Hiesinger, H., Bernhardt, H., Reiss, D., 2017. Topography of the Deuteronilus contact on Mars: evidence for an ancient water/mud ocean and long-wavelength topographic readjustments. Planet. Space Sci. 144, 49–70.
Kioka, A., Ashi, J., 2015. Episodic massive mud eruptions from submarine mud volcanoes examined through topographical signatures. Geophys. Res. Lett. 42 (20), 8406–8414.
Kite, E.S., Gao, P., Goldblatt, C., Mischna, M.A., Mayer, D.P., Yung, Y.L., 2017. Methane bursts as a trigger for intermittent lake-forming climates on post-Noachian Mars. Nat. Geosci. 10 (10), 737–740.
Kneissl, T., van Gasselt, S., Neukum, G., 2011. Map-projection-independent crater size-frequency determination in GIS environments—new software tool for ArcGIS. Planet. Space Sci. 59 (11–12), 1243–1254.
Komatsu, G., Okubo, C.H., Wray, J.J., Ojha, L., Cardinale, M., Murana, A., et al., 2016. Small edifice features in Chryse Planitia, Mars: assessment of a mud volcano hypothesis. Icarus 268, 56–75.
Li, C., Zhang, R., Yu, D., Dong, G., Liu, J., Geng, Y., et al., 2021. China's Mars exploration mission and science investigation. Space Sci. Rev. 217 (4), 57.
Liu, J., Michalski, J.R., Tan, W., He, H., Ye, B., Xiao, L., 2021. Anoxic chemical weathering under a reducing greenhouse on early Mars. Nat. Astron. 5 (5), 503–509.
Mayer, D.P., Kite, E.S., 2016. An integrated workflow for producing digital terrain models of Mars from CTX and HiRISE stereo data using the NASA ames stereo pipeline. In: LPSC XLVII, Abtr. #1241.
Mazzini, A., Etiope, G., 2017. Mud volcanism: an updated review. Earth-Sci. Rev. 168, 81–112.
McEwen, A.S., Eliason, E.M., Bergstrom, J.W., Bridges, N.T., Hansen, C.J., Delamere, W.A., et al., 2007. Mars Reconnaissance Orbiter's High Resolution Imaging Science Experiment (HiRISE). J. Geophys. Res., Planets 112 (E5).
McGill, G.E., Hills, L.S., 1992. Origin of giant Martian polygons. J. Geophys. Res., Planets 97 (E2), 2633–2647.
Meresse, S., Costard, F., Mangold, N., Masson, P., Neukum, G., 2008. Formation and evolution of the chaotic terrains by subsidence and magmatism: hydraotes chaos, Mars. Icarus 194 (2), 487–500.
Michael, G.G., Neukum, G., 2010. Planetary surface dating from crater size–frequency distribution measurements: partial resurfacing events and statistical age uncertainty. Earth Planet. Sci. Lett. 294 (3–4), 223–229.
Michalski, J.R., Onstott, T.C., Mojzsis, S.J., Mustard, J., Chan, Q.H.S., Niles, P.B., Johnson, S.S., 2018. The Martian subsurface as a potential window into the origin of life. Nat. Geosci. 11 (1), 21–26.
Mitrofanov, I.G., Litvak, M.L., Kozyrev, A.S., Sanin, A.B., Tret'yakov, V.I., Grin'kov, V.Y., et al., 2004. Soil water content on Mars as estimated from neutron measurements by the HEND instrument onboard the 2001 Mars Odyssey spacecraft. Sol. Syst. Res. 38 (4), 253–265.
Morgan, G., Putzig, N., Perry, M., Sizemore, H., Bramson, A., Petersen, E., et al., 2021. Availability of subsurface water-ice resources in the northern mid-latitudes of Mars. Nat. Astron. 5 (3), 230–236.
Mouginis-Mark, P., 1979. Martian fluidized crater morphology: variations with crater size, latitude, altitude, and target material. J. Geophys. Res., Solid Earth 84 (B14), 8011–8022.
Neukum, G., Ivanov, B.A., Hartmann, W.K., 2001. Cratering records in the inner solar system in relation to the lunar reference system. Space Sci. Rev. 96, 55–86.
Niemann, H., Lösekann, T., De Beer, D., Elvert, M., Nadalig, T., Knittel, K., et al., 2006. Novel microbial communities of the Haakon Mosby mud volcano and their role as a methane sink. Nature 443 (7113), 854–858.
Noguchi, R., Kurita, K., 2015. Unique characteristics of cones in Central Elysium Planitia, Mars. Planet. Space Sci. 111, 44–54.
Oehler, D.Z., Etiope, G., 2017. Methane seepage on Mars: where to look and why. Astrobiology 17 (12), 1233–1264.
Parker, T.J., Saunders, R.S., Schneeberger, D.M., 1989. Transitional morphology in West Deuteronilus Mensae, Mars: implications for modification of the lowland/upland boundary. Icarus 82 (1), 111–145.
Parker, T.J., Gorsline, D.S., Saunders, R.S., Pieri, D.C., Schneeberger, D.M., 1993. Coastal geomorphology of the Martian northern plains. J. Geophys. Res., Planets 98 (E6), 11061–11078.
Pedersen, G.B.M., Head, J.W., Wilson, L., 2010. Formation, erosion and exposure of Early Amazonian dikes, dike swarms and possible subglacial eruptions in the Elysium Rise/Utopia Basin Region, Mars. Earth Planet. Sci. Lett. 294 (3–4), 424–439.
Rodríguez, S.R., Morales-Barrera, W., Layer, P., González-Mercado, E., 2010. A quaternary monogenetic volcanic field in the Xalapa region, eastern trans-Mexican volcanic belt: geology, distribution and morphology of the volcanic vents. J. Volcanol. Geotherm. Res. 197 (1), 149–166.
Séjourné, A., Costard, F., Swirad, Z.M., Łosiak, A., Bouley, S., Smith, I., et al., 2019. Grid mapping the northern plains of Mars: using morphotype and distribution of ice-related landforms to understand multiple ice-rich deposits in Utopia Planitia. J. Geophys. Res., Planets 124, 483–503.
Skinner, J.A., Tanaka, K.L., 2007. Evidence for and implications of sedimentary diapirism and mud volcanism in the southern Utopia highland–lowland boundary plain, Mars. Icarus 186 (1), 41–59.
Sloan Jr, E.D., Koh, C.A., 2007. Clathrate Hydrates of Natural Gases. CRC Press.
Smith, D.E., Zuber, M.T., Frey, H.V., Garvin, J.B., Head, J.W., Muhleman, D.O., et al., 2001. Mars orbiter laser altimeter: experiment summary after the first year of global mapping of Mars. J. Geophys. Res., Planets 106 (E10), 23689–23722.
Smith, P.H., Tamppari, L.K., Arvidson, R.E., Bass, D., Blaney, D., Boynton, W.V., et al., 2009. H2O at the Phoenix landing site. Science 325 (5936), 58–61.
Soare, R.J., Conway, S.J., Williams, J-.P., Gallagher, C., McKeown, L.E., 2020. Possible (closed system) pingo and ice-wedge/thermokarst complexes at the mid latitudes of Utopia Planitia, Mars. Icarus 342, 113233.
Stillman, D.E., Grimm, R.E., 2011. Radar penetrates only the youngest geological units on Mars. J. Geophys. Res., Planets 116 (E3).
Stuurman, C.M., Osinski, G.R., Holt, J.W., Levy, J.S., Brothers, T.C., Kerrigan, M., Campbell, B.A., 2016. SHARAD detection and characterization of subsurface water ice deposits in Utopia Planitia, Mars. Geophys. Res. Lett. 43 (18), 9484–9491.
Tanaka, K.L., Skinner Jr., J.A., Hare, T.M., Joyal, T., Wenker, A., 2003. Resurfacing history of the northern plains of Mars based on geologic mapping of Mars global surveyor data. J. Geophys. Res., Planets 108 (E4).
Tanaka, K.L., Skinner, J.A., Hare, T.M., 2005. Geologic map of the northern plains of Mars. Nature 437 (7061), 991–994.
Tanaka, K.L., Skinner Jr., J.A., Dohm, J.M., Irwin III, R.P., Kolb, E.J., Fortezzo, C.M., Platz, T., Michael, G.G., Hare, T.M., 2014. Geologic map of Mars. U.S. Geological Survey Scientific Investigations Map 3292, scale 1:20,000,000, pamphlet 43 p. https://doi.org/10.3133/sim3292.
Thomas, P.C., Malin, M.C., Carr, M.H., Danielson, G.E., Davies, M.E., Hartmann, W.K., Ingersoll, A.P., James, P.B., McEwen, A.S., Soderblom, L.A., Veverka, J., 1999. Bright sand dunes on Mars. Nature 397, 592–594.
Wan, W.X., Wang, C., Li, C.L., Wei, Y., 2020. China's first mission to Mars. Nat. Astron. 4, 721.
Wu, B., Dong, J., Wang, Y., Li, Z., Chen, Z., Liu, W.C., Zhu, J., Chen, L., Li, Y., Rao, W., 2021. Characterization of the candidate landing region for Tianwen-1 – China's first mission to Mars. Earth Space Sci. 8, 6. https://doi.org/10.1029/2021EA001670.
Ye, P., et al., 2017. Mission overview and key technologies of the first Mars probe of China. Sci. China, Technol. Sci. 60, 649–657.
Yuan, B., Wang, C., Zou, M., Liu, Y., Lin, Y., Jia, Y., Chen, B., Jin, J., 2021. Experimental study on the durability of China's Mars rover's mobility system. J. Aerosp. Eng. 34 (5), 04021047.
Zhou, B., Shen, S., Lu, W., Li, Y., Liu, Q., Tang, C., Li, S., Fang, G., 2020. The Mars rover subsurface penetrating radar onboard China's Mars 2020 mission. Earth Planet. Phys. 4, 345–354.
Zou, Y.L., Zhu, Y., Bai, Y.F., Wang, L.G., Jia, Y.Z., Shen, W.H., et al., 2021. Scientific objectives and payloads of Tianwen-1, China's first Mars exploration mission. Adv. Space Res. 67 (2), 812–823.